Downloaded from jnm.snmjournals.org by on March 11, 2017. For personal use only.

^{18}F-Fluromisonidazole PET Imaging as a Biomarker for the Response to 5,6-Dimethylxanthenone-4-Acetic Acid in Colorectal Xenograft Tumors

Christoph Oehler[1,2], Joseph A. O'Donoghue[1], James Russell[1], Pat Zanzonico[1], Sylvie Lorenzen[3], C. Clifton Ling[1], and Sean Carlin[1,4]

[1]Department of Medical Physics, Memorial Sloan-Kettering Cancer Center, New York, New York; [2]Department of Radiation Oncology, University Hospital Zurich, Zurich, Switzerland; [3]Third Department of Internal Medicine (Hematology/Medical Oncology), Technical University of Munich, Munich, Germany; and [4]Department of Radiology, Memorial Sloan-Kettering Cancer Center, New York, New York

The aim of this study was to evaluate ^{18}F-fluromisonidazole (^{18}F-FMISO) PET for monitoring the tumor response to the antivascular compound 5,6-dimethylxanthenone-4-acetic acid (DMXAA; vadimezan). **Methods:** ^{18}F-FMISO PET was performed 3 h before and 24 h after treatment with DMXAA (20 mg/kg) in mice bearing HT29 xenograft tumors. Pimonidazole was coadministered with the first ^{18}F-FMISO injection, and 2-(2-nitro-1H-imidazol-1-yl)-*N*-(2,2,3,3,3-pentafluoropropyl)acetamide (EF5) was coadministered with the second one. Hoechst 33342 was administered 5 min before sacrifice. Digital autoradiograms of tumor sections were acquired; this acquisition was followed by immunofluorescence microscopic visualization of pimonidazole, EF5, the Hoechst 33342, CD31, and α-smooth muscle actin. **Results:** DMXAA treatment resulted in a marked reduction in the ^{18}F-FMISO mean standardized uptake value (SUV_{mean}) in approximately half of the treated tumors. The reduction in SUV_{mean} correlated with a decrease in the fraction of tumor area staining positive for both EF5 and pimonidazole. Compared with untreated controls, tumors with decreasing SUV_{mean} had significantly fewer perfused microvessels. **Conclusion:** ^{18}F-FMISO PET could distinguish between different tumor responses to DMXAA treatment. However, a reduction in ^{18}F-FMISO SUV_{mean} after DMXAA treatment was indicative of reduced perfusion and therefore delivery of ^{18}F-FMISO, rather than a reduction in tumor hypoxia.

Key Words: PET; ^{18}F-FMISO; hypoxia; DMXAA; antivascular treatment

J Nucl Med 2011; 52:437–444
DOI: 10.2967/jnumed.110.081372

Vasculature-targeted therapies, increasingly used as a component of integrated oncologic treatment for such diverse tumor types as colon cancer, lung cancer, breast cancer, B-cell lymphoma, and myelogenous leukemia, have been shown to improve treatment response and survival (*1,2*). Classes of agents that exert antitumor effects either through the inhibition of tumor blood vessel development (antiangiogenic agents) or through the functional disruption of established vessels (tumor vasculature-disrupting agents [VDAs]) have been identified.

Several VDAs are currently undergoing clinical trials for the treatment of various malignancies (reviewed by McKeage and Baguley (*3*)). Of these, 5,6-dimethylxanthenone-4-acetic acid (DMXAA; ASA404; vadimezan) is the most extensively studied in the clinical setting. It is the first tumor VDA entering a phase III trial (for lung cancer), after having shown promise in phase II clinical trials for lung cancer (*4*) and prostate cancer (*5*). DMXAA induces rapid endothelial cell (EC) apoptosis, occlusion of and decreased perfusion in preexisting tumor vessels, and the subsequent development of central hemorrhagic necrosis (reviewed by Baguley and Siemann (*6*)). Major irreversible reductions in tumor perfusion have been observed within 6 h of DMXAA administration in murine xenograft models (*7,8*). Treatment with VDAs also commonly results in a residual viable rim of proliferating cells at the tumor periphery, presumably deriving oxygen and nutrients from surrounding normal tissue vasculature (*9,10*).

Given the mechanism of action of VDAs and their potential for interaction with other therapies, it is likely that the integration and scheduling of such combined treatments will need to be optimized on a disease-specific and, possibly, patient-specific basis. To facilitate such optimization, conventional volumetric measures for monitoring responses to therapies, such as RECIST (Response Evaluation Criteria in Solid Tumors), may be inadequate (*11,12*). There is increasing enthusiasm for the use of functional imaging to monitor the tumor response, with a view toward the possibility of individualized response-adapted treatment (*13*). For example, gadolinium contrast–enhanced dynamic MRI has been used to evaluate the effects of DMXAA treatment (*9,14,15*). This technique yields information

Received Aug. 23, 2010; revision accepted Dec. 2, 2010.
For correspondence or reprints contact: Sean Carlin, Department of Medical Physics, MSKCC, 1275 York Ave., New York, NY 10021.
E-mail: carlins@mskcc.org
COPYRIGHT © 2011 by the Society of Nuclear Medicine, Inc.

Downloaded from jnm.snmjournals.org by on March 11, 2017. For personal use only.

about tumor vascular functionality but does not directly assess tumor hypoxia or necrosis. Because tumor vasculature and oxygenation status are related, VDA treatment may result in reduced delivery of chemotherapeutic agents together with an increase in tumor hypoxia and a consequent decrease in radiation sensitivity. Noninvasive imaging of such changes is therefore of particular interest in the context of clinical studies that combine DMXAA with radiation or chemotherapy (*16–18*).

Several potential hypoxia tracers are now available for use as PET agents (*19*). Of these, ^{18}F-fluoromisonidazole (^{18}F-FMISO) has been the most extensively studied and validated (*20,21*). The aim of the present study was to investigate whether ^{18}F-FMISO PET could yield tumor response data in mice treated with DMXAA.

MATERIALS AND METHODS

Cell Lines and Animal Models

HT29 human colorectal adenocarcinoma cells were obtained from the American Type Culture Collection. Cells were maintained in McCoy 5A modified medium (Life Sciences) supplemented with 10% fetal bovine serum (Gemini) and 1% penicillin–streptomycin solution (Invitrogen). Cells were grown at 37°C in a humidified CO_2 incubator. Exponentially growing cells were harvested with 0.05% trypsin plus ethylenediaminetetraacetic acid, washed, and suspended in phosphate-buffered saline (PBS).

All in vivo experiments were performed with 6- to 8-wk-old female athymic NCr-*nu/nu* mice purchased from the National Cancer Institute–Frederick Cancer Research Institute. Mice were maintained and used in accordance with institutional guidelines, and experimental protocols were approved by the institutional animal care and use committee. For experimental tumors, 5×10^6 cells suspended in 0.2 mL of PBS were subcutaneously transplanted into the dorsum of the right or left hind limb. Imaging experiments were initiated when the tumors reached approximately 12 mm in diameter.

DMXAA Treatment

DMXAA was obtained from Sigma-Aldrich, dissolved in dimethyl sulfoxide, and further diluted in PBS to a final concentration of 2.5 mg/mL immediately before injection. Treated animals were administered DMXAA at 20 mg/kg by intraperitoneal injection. Control animals were administered vehicle only, that is, the same volumes and concentrations of dimethyl sulfoxide and PBS as for the DMXAA-treated animals. In all, there were 12 evaluable tumors in the treated group and 7 in the control group.

^{18}F-FMISO Small-Animal PET

^{18}F-fluoride was produced on the Memorial Sloan-Kettering Cancer Center cyclotron (TR19/9; EBCO Technologies, Inc.) with previously described techniques (*22*). ^{18}F-FMISO was prepared as previously reported (*23*). ^{18}F-FMISO PET was performed on mice bearing xenograft tumors before (3 h) and after (24 h) treatment with DMXAA. Mice were anesthetized for ^{18}F-FMISO administration and scanning by breathing 2% isoflurane in air. Approximately 37 MBq (1 mCi) of ^{18}F-FMISO was administered via tail vein injection. Mice were imaged in a prone position with either an R4 or a Focus 120 dedicated microPET scanner (Concorde Microsystems Inc.), an energy window of 350–700 keV, and a coincidence timing window of 6 ns. Images were acquired over a period of 10 min at 80 min after administration.

For facilitating the differential immunohistochemical (IHC) localization of tumor hypoxia, pimonidazole HCl (Hypoxyprobe-1; Natural Pharmacia International Inc.; 80 mg/kg in physiologic saline) was coadministered with ^{18}F-FMISO before DMXAA treatment, and 2-(2-nitro-1H-imidazol-1-yl)-*N*-(2,2,3,3,3-pentafluoropropyl)acetamide (EF5; provided by Dr. Cameron J. Koch, University of Pennsylvania; 24 mg/kg in PBS) was coadministered with ^{18}F-FMISO after DMXAA treatment. After the final ^{18}F-FMISO imaging session, a fluorescent dye (Hoechst 33342 trihydrochloride; Sigma; 40 mg/kg; 1 mg in 100 μL of physiologic saline) was injected 5 min before sacrifice.

PET Image Analysis

The list-mode data were sorted into 2-dimensional histograms by Fourier rebinning, and images were reconstructed by filtered backprojection with a ramp filter that had a cutoff frequency equal to the Nyquist frequency in either a $128 \times 128 \times 64$ matrix (R4) or a $128 \times 128 \times 94$ matrix (Focus 120). The image data were corrected for nonuniformity of the scanner response, dead time count losses, and physical decay to the time of injection, but no correction was applied for attenuation, scatter, or partial-volume averaging. The counting rates in the reconstructed images were converted to activity concentration and subsequently to percentage injected dose per gram of tissue (%ID/g) with a system calibration factor (kBq/mL/cps/voxel) derived from imaging of a mouse-size phantom filled with a uniform aqueous solution of ^{18}F.

Images for each tumor or animal were visually examined by use of ASIProVM (Concorde Microsystems) with window and level settings adjusted for maximum tumor visibility. The images were assessed qualitatively, and a report on the salient features of the activity distribution within the tumor was produced. A region of interest was manually drawn to circumscribe the whole tumor on a midtumor coronal slice, and the mean %ID/g within the region of interest was obtained. This value was converted to a mean standardized uptake value (SUV_{mean}) with the formula [%ID/g × body mass (g)]/100 (*24*). The maximum-intensity pixel (SUV_{max}) from each region of interest was also determined. To compare changes in ^{18}F-FMISO uptake between DMXAA-treated and control groups, we used the parameter ΔSUV_{mean}, which was calculated as the SUV_{mean} before treatment minus the SUV_{mean} after treatment.

Preparation of Frozen Tumor Sections

After the last imaging session, animals were sacrificed and tumors were excised, embedded in mounting medium (O.C.T. Compound; Sakura Finetek), and frozen on dry ice. Sets of contiguous frozen tissue sections were cut at a thickness of 6 μm on an HM500 cryostat microtome (Microm International GmbH) and collected on glass microscope slides.

Autoradiography

For facilitating comparison of the spatial distributions of the PET tracer and IHC markers at the microscopic level, digital autoradiography (DAR) was performed on tissue sections prepared as described earlier. Sections were placed in a film cassette against a phosphor imaging plate (Fujifilm BAS-MS2325; Fuji Photo Film). Phosphor imaging plates were read at a resolution of 50×50 μm with a BAS-1800II Bio-Imaging Analyzer (Fujifilm Medical Systems).

IHC Staining for Hypoxia and Vessels

IHC staining for pimonidazole and EF5 was performed on the same sections as those used for autoradiography as described

Downloaded from jnm.snmjournals.org by on March 11, 2017. For personal use only.

previously (*25*). Staining was performed at room temperature unless stated otherwise. Contiguous adjacent sections were then stained for the vascular markers CD31 and α-smooth muscle actin (α-SMA) as follows. After sections were fixed in 4% paraformaldehyde solution for 12 min, blocking in Superblock/PBS (Thermo Scientific) for 30 min was performed. Next, sections were sequentially incubated in rat antimouse CD31 antibody (clone MEC13.3; BD Biosciences) for 1 h, biotinylated rabbit antirat IgG (Invitrogen) for 1 h, Elite ABC reagent (R.T.U. VECTASTAIN Kit; Vector Laboratories, Inc.) for 30 min, and AlexaFluor 488 tyramide (Invitrogen) for 15 min. For the detection of α-SMA, the same sections were then stained with anti–α-SMA-Cy3 antibody (clone 1A4; Sigma-Aldrich) diluted in Superblock/PBS.

Digital images of the distributions of pimonidazole, EF5, CD31, α-SMA, and Hoechst 33342 in tumor sections were acquired at a magnification of ×100 by use of a fluorescence microscope (Diaphot 300; Nikon) equipped with a computer-controlled motorized stage and a digital Coolsnap EZ camera (Photometrics) for image capture. After fluorescence images were acquired, tumor sections were stained with hematoxylin and eosin and imaged by light microscopy. Composite images of whole tumor sections were obtained by "stitching" together individual microscopic images with Image-Pro software (Image-Pro Plus, version 7.0; Adobe Systems).

Quantification of IHC Staining

Image processing was performed with Photoshop software (version 7.0; Adobe Systems). Tumor area was determined by manual delineation of tumor boundaries, and then the total number of pixels within the marked region was determined. Tumor area was calculated with the appropriate calibration factor (micrometers per pixel) for the objective used. Necrotic areas in tumor sections (identified from hematoxylin- and eosin-stained images) were masked and excluded from subsequent analysis.

The fractions of tumor areas positive for pimonidazole, EF5, and Hoechst 33342 were determined by use of the method of Li et al. (*26*). In brief, thresholds for pimonidazole and EF5 positivity were defined with respect to the pimonidazole and EF5 fluorescence intensities observed in tumor regions clearly positive for Hoechst 33342 fluorescence. Similarly, the threshold for Hoechst 33342 positivity was defined with respect to the Hoechst 33342 fluorescence intensity observed in tumor regions clearly positive for EF5 fluorescence. If the fluorescence intensity in a pixel was greater than the relevant threshold value, then the pixel was classified as positive for the marker in question. For examining the colocalization of pimonidazole and EF5, binary images were generated on the basis of the positivity thresholds. Pixels positive for pimonidazole and for EF5 were assigned values of 130 and 90, respectively, on an 8-bit grayscale of 0–255. A summed image containing pixels with 4 possible values—0, 90, 130, and 220—was then generated. The fraction of pixels within a section with a value of 220 represented the fraction of the tumor positive for both markers.

Immunofluorescence images of CD31, α-SMA, and Hoechst 33342 were analyzed with CellProfiler software (Broad Institute; freeware available at http://www.cellprofiler.org/index.htm). (Analysis pipelines are available on request.) For each tumor section, 10 high-power microscope fields (0.162 mm^2 each) within areas containing no visible necrosis were assessed. Vascular structures were defined as those staining positive for either CD31 or α-SMA. Perfused vascular structures were defined as vascular structures also staining positive for Hoechst 33342. Each vascular structure was also assessed for positivity for both CD31 and α-SMA, allowing an analysis of vascular maturity. Object identification algorithms were calibrated by visual inspection and counting.

Statistical Analysis

Statistical comparisons of DMXAA-treated and control groups were performed with unpaired Student *t* tests (2-tailed). A *P* value of less than 0.05 was regarded as being statistically significant.

RESULTS

Effect of DMXAA on ^{18}F-FMISO Activity Distribution in PET Images

At the time of treatment, the mean tumor volume was 535 mm^3 (SD, 288 mm^3) ($n = 19$). The difference between SUV_{mean} of pretreatment scans and SUV_{mean} of posttreatment scans (ΔSUV_{mean}) was determined for each tumor; average values of this parameter for DMXAA-treated and control groups are shown in Table 1. There was no significant difference between DMXAA-treated and control groups in terms of ΔSUV_{mean} ($P > 0.5$). However, examination of the PET images showed that the responses to DMXAA were highly variable among tumors. Some tumors exhibited a discernible decrease in ^{18}F-FMISO uptake, whereas others showed little change or even an increase. We decided to investigate whether the underlying causes of the divergent responses could be identified.

On the basis of ΔSUV_{mean}, we designated 2 groups of DMXAA-treated tumors: DMXAA-1 (ΔSUV_{mean}, ≥ 0) and DMXAA-2 (ΔSUV_{mean}, < 0). Figure 1 shows the SUV_{mean} of each tumor at baseline and at 24 h after treatment for the control group (which received vehicle only) (Fig. 1A) and for the DMXAA-1 (Fig. 1B) and DMXAA-2 (Fig. 1C) groups. Summary statistics for ΔSUV_{mean} in the DMXAA-1 and DMXAA-2 groups are shown in Table 1. *P* values are provided for completeness, but no statistical interpretations can be drawn because of the selection procedure used. Qualitatively, tumors in the DMXAA-2 group invariably showed a distinct loss of ^{18}F-FMISO activity in the center of the tumor. This finding was not seen in control tumors or tumors in the DMXAA-1 group. A similar analysis with SUV_{max} resulted in an identical group distribution, with the exception of a single tumor (Supplemental Fig. 1) (supplemental materials are available online only at http://jnm.snmjournals.org).

Figures 2A and 2B show examples of pretreatment and posttreatment ^{18}F-FMISO PET images, respectively, for a tumor in the DMXAA-2 group.

Correspondence of ^{18}FMISO Distribution in PET Images with IHC Hypoxia Markers

In all cases, DAR images of ^{18}F-FMISO obtained from frozen tumor sections appeared grossly similar to the corresponding posttreatment ^{18}F-FMISO small-animal PET images (Figs. 2B and 2D). At the histologic level, the nitroimidazole hypoxia tracer EF5 colocalized with ^{18}F-FMISO administered after treatment (Figs. 2B and 2D). The intra-

Downloaded from jnm.snmjournals.org by on March 11, 2017. For personal use only.

TABLE 1
Changes in ^{18}F-FMISO SUV_{mean} After DMXAA Treatment

Treatment group (*n*)	Average ΔSUV_{mean} (SD)	*P* for DMXAA-treated group vs. control group
Control (7)	−0.017 (0.253)	
DMXAA total (12)	−0.19 (0.67)	0.52
DMXAA-1 (7)	0.15 (0.61)	0.51
DMXAA-2 (5)	−0.68 (0.42)	0.0065

tumoral distribution of pimonidazole also appeared grossly similar to the pretreatment ^{18}F-FMISO distribution in PET images (Figs. 2A and 2C). In untreated tumors, the distributions of pimonidazole, EF5, and ^{18}F-FMISO appeared similar (Fig. 3 and Supplemental Fig. 2). We concluded from these observations that the distribution of ^{18}F-FMISO (assessed by either PET or DAR) was representative of the distributions of the histologic hypoxia markers in all tumors studied, regardless of the treatment group or response type.

Effect of DMXAA on Hypoxia and Perfusion Markers

For tumors in the control and DMXAA-1 groups, EF5 and pimonidazole staining localized primarily to central tumor regions; less uptake was observed at the tumor periphery. In contrast, for tumors in the DMXAA-2 group, EF5 and pimonidazole typically displayed different localization patterns. EF5-positive regions were localized predominantly at the tumor rim and were conspicuously absent from the center. Visual examination also indicated that for tumors in the DMXAA-2 group, the perfusion marker Hoechst 33342 was localized exclusively at the rim; this distribution was similar at a gross level to the distribution of EF5. Examples are shown in Figure 3 and Supplemental Figure 3.

Effect of DMXAA on Tumor Vasculature

The effect of DMXAA on tumor vasculature was assessed by immunofluorescence staining for the EC marker CD31 (platelet endothelial cell adhesion molecule-1) and the pericyte marker α-SMA (Supplemental Fig. 3). Qualitatively, tumors in both the control and the DMXAA-1 groups showed CD31-positive vessellike circular structures concordant with the α-SMA pattern. In contrast, tumors in the DMXAA-2 group showed fewer CD31-positive structures with a more heterogeneous pattern of α-SMA positivity. These observations indicated that DMXAA-treated tumors displayed highly variable responses at the microscopic level, consistent with the PET findings.

Quantitative Changes in Hypoxia and Perfusion Markers and Correlation with ^{18}F-FMISO PET

Using coregistered images and applying appropriate intensity thresholds, we determined the fractions of tumor areas staining positive for Hoechst 33342, EF5, and pimonidazole. The fractions of tumor area staining positive for Hoechst 33342 were 20% (SD, 9%) in control tumors, 25% (SD, 10%) ($P = 0.28$) in DMXAA-1 tumors, and 6% (SD, 4%) ($P = 0.01$) in DMXAA-2 tumors (Fig. 4A). The fractions of tumor area staining positive for pimonidazole (administered before DMXAA treatment) were similar in control tumors (27% [SD, 13%]) and treated tumors (DMXAA-1: 27% [SD, 7%]; DMXAA-2: 35% [SD, 7%]; $P > 0.05$ in all cases) (Fig. 4B). The fractions of tumor area staining positive for EF5 (administered after DMXAA treatment) decreased to 15% (SD, 4%) ($P < 0.05$) in DMXAA-2 tumors but remained unchanged ($P > 0.5$) in control tumors (26% [SD, 10%]) and DMXAA-1 tumors (28% [SD, 6%]) (Fig. 4C).

In terms of hypoxia marker colocalization, the fractions of pimonidazole-positive areas that were also positive for EF5 were 63% (SD, 14%) in the control group, 74% (SD, 15%) in the DMXAA-1 group ($P = 0.21$), and 33% (SD, 1%) in the DMXAA-2 group ($P = 0.0006$) (Fig. 4D). A scatterplot of the percentage of hypoxia marker colocalization versus the ΔSUV_{mean} for all (treated and control) tumors (Fig. 5) revealed a clear positive correlation ($r^2 = 0.7$). Taken together, these data demonstrate the consistency of assessing DMXAA-induced changes in the distribution of tumor hypoxia markers by sequential noninvasive ^{18}F-FMISO small-animal PET imaging and IHC staining of excised tumor sections.

Quantitative Changes in Tumor Vascular Function and Correlation with ^{18}F-FMISO PET

Quantification of tumor microvasculature was performed with automated object recognition software (CellProfiler). We separately identified immature microvessels (CD31 positive and α-SMA negative [CD31+/α-SMA−]) and mature microvessels containing ECs (CD31 positive and α-SMA positive [CD31+/α-SMA+]) or lacking ECs

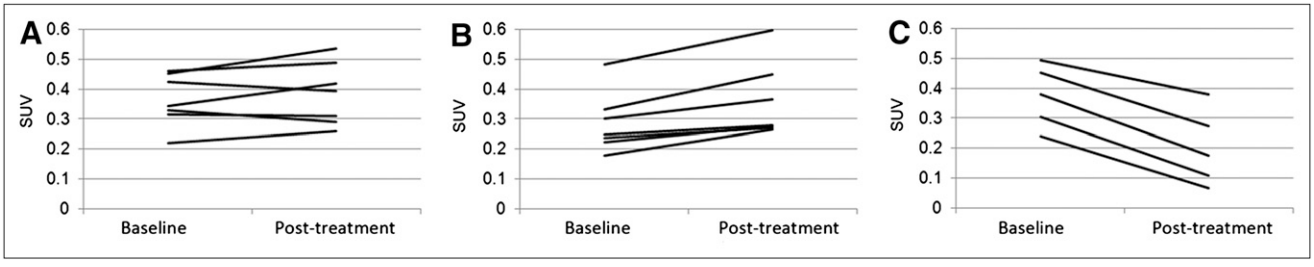


FIGURE 1. ^{18}F-FMISO SUV_{mean} before and after treatment with DMXAA. (A) Control tumors treated with vehicle only ($n = 7$). (B) DMXAA-treated tumors in which SUV did not decrease ($n = 7$) (DMXAA-1). (C) DMXAA-treated tumors in which SUV did decrease ($n = 5$) (DMXAA-2).

Downloaded from jnm.snmjournals.org by on March 11, 2017. For personal use only.

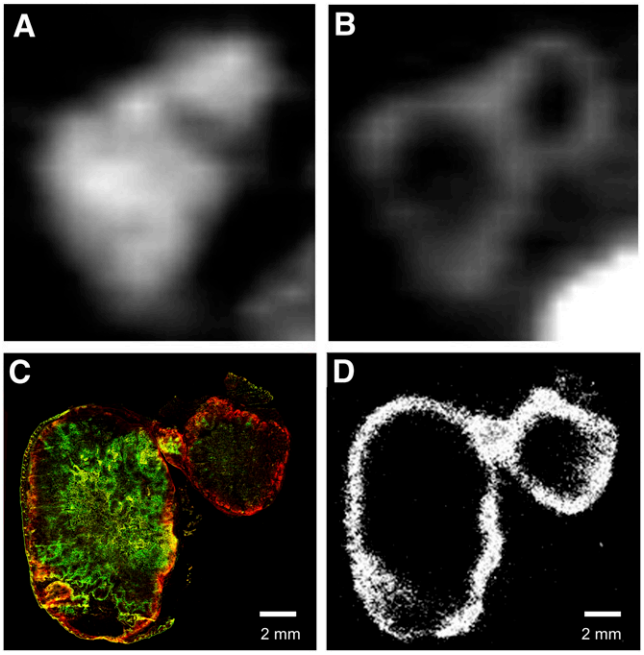


FIGURE 2. Pretreatment and posttreatment images of tumor with SUV_{mean} decrease. (A and B) Midcoronal slices of ^{18}FMISO small-animal PET images before (A) and after (B) treatment with DMXAA. (C) Composite fluorescence image of pimonidazole (green) and EF5 (red). Yellow indicates regions of colocalization. (D) DAR of same tumor section visualizing ^{18}F-FMISO activity.

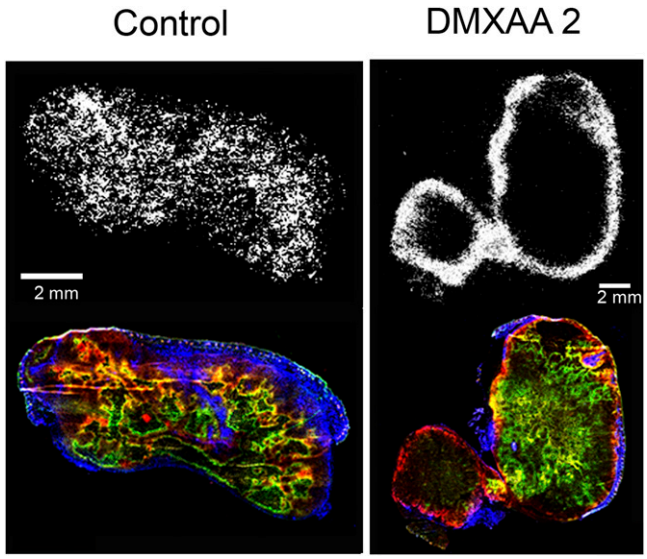


FIGURE 3. Comparison of ^{18}F-FMISO DAR and IHC staining of tumor hypoxia and vasculature. Top row shows ^{18}F-FMISO DAR; bottom row shows composite fluorescence image of Hoechst 33342 (blue), pimonidazole (green), and EF5 (red).

(CD31 negative and α-SMA positive [CD31−/α-SMA+]). Additionally, each vascular structure was classified as perfused or nonperfused on the basis of Hoechst 33342 fluorescence. The total numbers of microvessels (CD31+/SMA+, CD31+/SMA−, and CD31−/SMA+) in control and treated tumors were similar, regardless of ΔSUV_{mean} (Table 2). However, tumors in the DMXAA-2 group (i.e., with an ΔSUV_{mean} of <0) had a smaller number of mature microvessels containing ECs ($P = 0.02$) and a nonsignificant trend toward a larger number of mature microvessels lacking ECs ($P = 0.08$) (Table 2). No significant difference in structure sizes in the groups was found. Although there was little difference in the total numbers of microvessels, a clear difference was observed in the percentages of perfused vessels (Table 2). The fractions of perfused microvessels were 24% (SD, 9%) in control tumors, 36% (SD, 9%) in DMXAA-1 tumors ($P = 0.03$), and 4% (SD, 3%) in DMXAA-2 tumors ($P = 0.001$). The trends observed were similar, regardless of the CD31 or α-SMA status of the vessels examined. A scatterplot of the percentage of microvessels perfused versus the ΔSUV_{mean} for all (treated and

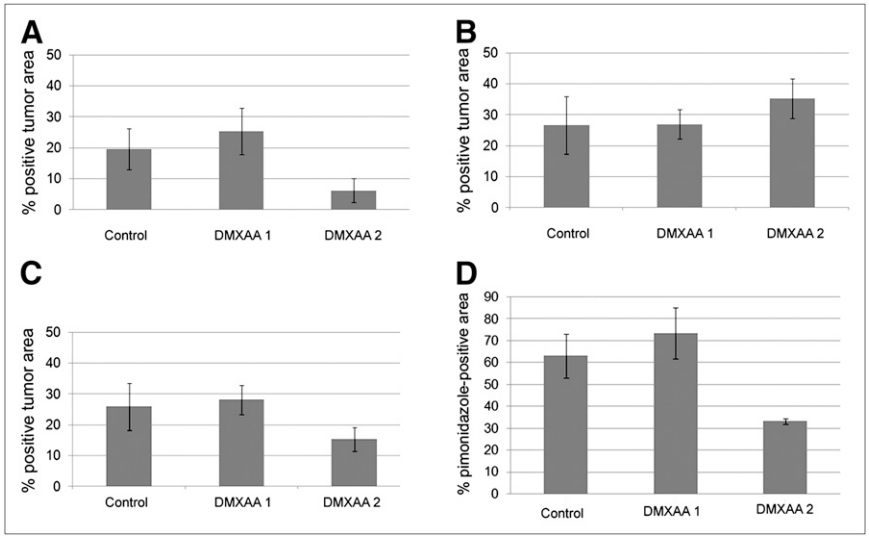


FIGURE 4. Fractions of positive perfusion and hypoxia. (A–C) Fractions of viable tumor area positive for Hoechst 33342 (A), pimonidazole (B), and EF5 (C). (D) Percentage of pimonidazole-positive viable tumor area also positive for EF5.

Downloaded from jnm.snmjournals.org by on March 11, 2017. For personal use only.

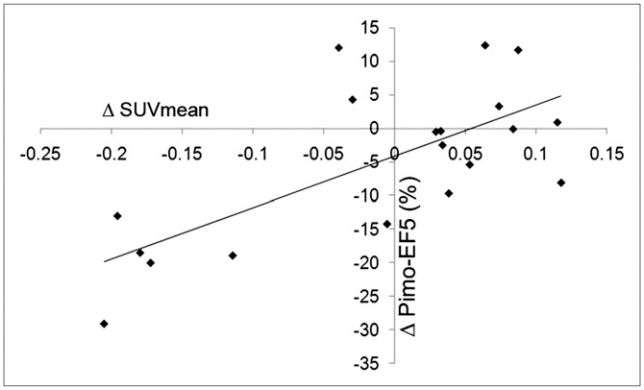


FIGURE 5. Scatterplot of pimonidazole (Pimo)–EF5 colocalization vs. ΔSUV_{mean}. Regression line shows that r^2 was 0.7.

control) tumors (Fig. 6) revealed a positive correlation ($r^2 = 0.6$).

These data suggest that the decrease in ^{18}F-FMISO activity observed for tumors in the DMXAA-2 group may have been produced by functional disruption of the tumor microvasculature, resulting in decreased radiotracer delivery. These data also suggest that the increase in SUV_{mean} observed for tumors in the DMXAA-1 group may reflect an underlying increase in vessel perfusion or permeability, which is also consistent with the mechanism of action of DMXAA (Fig. 4A). It is not possible to draw definitive conclusions regarding changes in tumor hypoxia without direct measurement of pO_2 with oxygen-sensitive probes. However, in our experience with HT29 xenograft tumors, regions with a high level of vascular perfusion are generally inversely correlated with regions of tumor hypoxia (*26*). We conclude from our data that the changes in tumor ^{18}F-FMISO uptake observed after DMXAA administration are governed primarily by altered vascular delivery of ^{18}F-FMISO, rather than underlying changes in tumor hypoxia.

DISCUSSION

Noninvasive functional imaging for monitoring tumor responses after targeted therapies is of increasing clinical interest. In particular, a means of assessing the growing number of drugs that affect tumor vascularity and function could allow for patient-specific optimization of treatment protocols as well as for appropriate scheduling of combined-modality therapies (*27*). Given the close relationship between tumor perfusion and tumor hypoxia, we investigated the use of the hypoxia radiotracer ^{18}F-FMISO as a means of evaluating the effects of the clinically relevant antivascular agent DMXAA (vadimezan) in a murine xenograft tumor model.

We observed significant variability in tumor responses to DMXAA treatment. Our observations were generally consistent when either SUV_{mean} or SUV_{max} was used to determine ^{18}F-FMISO uptake (Supplemental Fig. 1). In terms of noninvasive ^{18}F-FMISO PET, some tumors exhibited a decrease in ^{18}F-FMISO uptake, whereas others showed little change or even an increase. A possible interpretation of the latter observation is that reduced ^{18}F-FMISO uptake reflected a decrease in tumor hypoxia. However, our further studies suggest that this possibility is unlikely.

For purposes of analysis, we categorized the tumor response to DMXAA as either DMXAA-1 (no change or increasing SUV_{mean}) or DMXAA-2 (decreasing SUV_{mean}). At the histologic level, DMXAA-1 corresponded to no apparent vascular disruption with stable or increased perfusion, whereas DMXAA-2 corresponded to significant vascular disruption with decreased perfusion. This characterization suggests that the DMXAA-2 response describes a tumor that would be more (rather than less) likely to be hypoxic, with the decrease in ^{18}F-FMISO uptake reflecting diminished vascular delivery of the tracer to the tumor. This interpretation is supported by our similar findings for the hypoxia markers pimonidazole and EF5, assessed by immunofluorescence microscopy of excised tumor sections. Analysis of ^{18}F-FMISO PET images for the DMXAA-2 group revealed a characteristic loss of ^{18}F-FMISO uptake in the central tumor region but not in the tumor rim. This pattern broadly matched the pattern of blood perfusion, assessed on the basis of the distribution of Hoechst 33342 in tumor sections. The opposite pattern was generally observed in the control and DMXAA-1 groups, with greater uptake in the central tumor region than in the tumor rim.

TABLE 2
Quantitative Changes in Vasculature and Perfusion After DMXAA Treatment

Treatment Group	Total structures				CD31+/α-SMA+ structures				CD31+/α-SMA− structures				CD31−/α-SMA+ structures			
	No. (SD)	*P*	Average % perfused fraction (SD)	*P*	No. (SD)	*P*	Average % perfused fraction (SD)	*P*	No. (SD)	*P*	Average % perfused fraction (SD)	*P*	No. (SD)	*P*	Average % perfused fraction (SD)	*P*
Control	327 (44)		24 (9)		133 (29)		34 (10)		60 (32)		30 (12)		134 (41)		11 (7)	
DMXAA-1	343 (85)	0.7	36 (9)	0.03	129 (42)	0.8	53 (15)	0.01	49 (34)	0.5	44 (28)	0.3	165 (94)	0.4	21 (11)	0.06
DMXAA-2	319 (97)	0.9	4 (3)	0.001	81 (34)	0.02	7 (10)	0.001	55 (36)	0.8	4 (5)	0.001	182 (43)	0.08	2 (2)	0.02

Data show total numbers and percentages of perfused immature microvessels (CD31+/α-SMA−) and mature microvessels containing ECs (CD31+/α-SMA+) or lacking ECs (CD31−/α-SMA+). *P* values are for comparisons with control tumors.

Downloaded from jnm.snmjournals.org by on March 11, 2017. For personal use only.

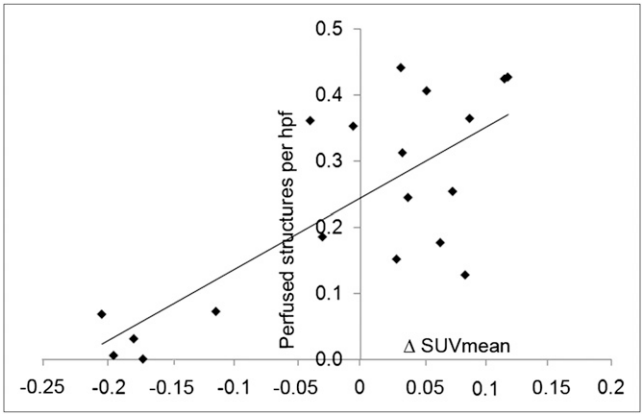


FIGURE 6. Scatterplot of fraction of perfused microvessels vs. ΔSUV_{mean}. Regression line shows that r^2 was 0.585. hpf = high-power field.

These findings have important implications for the use of vasculature-borne molecular imaging agents in the assessment of responses to therapies that have a direct effect on tumor vasculature. Changes in the apparent uptake of a given imaging agent cannot be assumed to directly reflect its molecular target, unless tracer delivery is also considered. Although the use of simple metrics such as ΔSUV_{mean} may provide an indirect indication of a gross pharmacologic effect, care must be taken in the interpretation of the data. In this particular case, reduced SUV_{mean} and loss of central tumor ^{18}F-FMISO uptake could erroneously be interpreted as an indication of tumor reoxygenation and reduction in the hypoxic fraction.

Possible means for overcoming these problems include the concurrent use of gadolinium contrast–enhanced dynamic MRI to directly assess tumor vascular functionality or the use of compartmental modeling of dynamic ^{18}F-FMISO PET data. MRI-based techniques were previously used to evaluate the tumor vascular response to DMXAA (*28,29*), but these techniques provided no information regarding tumor hypoxia or any discrimination between hypoxic and necrotic tumor regions. We are currently exploring the use of combined dynamic ^{18}F-FMISO PET and dynamic contrast-enhanced MRI to clarify these issues in model systems (*30*).

The use of dynamic ^{18}F-FMISO PET in a clinical setting is in the preliminary stage, but early indications are that such an approach is feasible and may provide more information than single-time-point static imaging (*31,32*).

A previous study reported that DMXAA and combretastatin A4 phosphate markedly inhibited blood flow and increased the uptake of the hypoxia tracer ^{99m}Tc-HL-91 in a range of tumor model systems (*8*). Important differences between that study and the present study are that the antivascular agent and the hypoxia tracer were coadministered and uptake was assessed after 3 h in the previous study. In such a scheme, the initial vascular delivery of the hypoxia tracer would not be impeded by vascular disruption, a fact that may explain the observed increase in absolute uptake. However, another possible explanation is that the increase in uptake was partly due to impaired clearance of unbound hypoxia tracer from the tumor because of the deterioration of vascular function over the 3-h experimental time frame. This information highlights the potential benefit of compartmental modeling for identifying the relative contributions of tracer delivery, clearance, and specific uptake.

The correlations among ^{18}F-FMISO, EF5, and pimonidazole distributions in the present study were made with a single xenograft tumor model. Previous studies indicated that tumor microarchitecture can have a significant influence on the relative distributions of ^{18}F-FMISO and pimonidazole (*33*). HT29 xenograft tumors display a characteristic "ribbonlike" pattern of hypoxia, which was previously shown to result in good correlations among 2-nitroimidazole hypoxia tracers in several models. The influence of differences in tumor microarchitecture on ^{18}F-FMSIO distribution after DMXAA treatment was not addressed in the present study and warrants further investigation.

CONCLUSION

The use of noninvasive ^{18}F-FMISO PET to assess tumor responses to antivascular agents, such as DMXAA, is feasible and reflects microenvironmental changes. However, care must be taken in the interpretation of such images because altered vascular function can have a significant effect on radiotracer delivery and intratumoral distribution independent of local hypoxia status. Dynamic imaging protocols may better characterize the interrelationships of tumor hypoxia and vascular perfusion in response to vasculature-modifying therapies.

ACKNOWLEDGMENTS

We thank the Memorial Sloan-Kettering Cancer Center (MSKCC) Cyclotron-Radiochemistry Core Facility for assistance with isotope production and radiochemical synthesis. Technical services provided by the MSKCC Small-Animal Imaging Core Facility, supported in part by NIH Small-Animal Imaging Research Program (SAIRP) grant R24 CA83084 and NIH Center grant P30 CA08748, are gratefully acknowledged. The latter grant also partially supports the MSKCC Research Animal Resource Center. We also thank Dr. Cameron J. Koch, Department of Radiation Oncology, School of Medicine, University of Pennsylvania, for supplying EF5 and Valerie Longo for expertise and assistance with PET imaging. This study was supported by National Institutes of Health grants R01 CA84596 and P01 CA115675; in part by generous grants from the Walter and Gertrud Siegenthaler Foundation and the Swiss Cancer League; and in part by generous grants from the Byrne Foundation and the Geoffrey Beene Cancer Research Foundation.

REFERENCES

1. Sato M, Arap W, Pasqualini R. Molecular targets on blood vessels for cancer therapies in clinical trials. *Oncology (Williston Park).* 2007;21:1346–1352.

Downloaded from jnm.snmjournals.org by on March 11, 2017. For personal use only.

2. Gridelli C, Rossi A, Maione P, et al. Vascular disrupting agents: a novel mechanism of action in the battle against non-small cell lung cancer. *Oncologist.* 2009;14:612–620.
3. McKeage MJ, Baguley BC. Disrupting established tumor blood vessels: an emerging therapeutic strategy for cancer. *Cancer.* 15;116:1859–1871.
4. McKeage MJ, Reck M, Jameson MB, et al. Phase II study of ASA404 (vadimezan, 5,6-dimethylxanthenone-4-acetic acid/DMXAA) 1800mg/m^2 combined with carboplatin and paclitaxel in previously untreated advanced non-small cell lung cancer. *Lung Cancer.* 2009;65:192–197.
5. McKeage MJ. The potential of DMXAA (ASA404) in combination with docetaxel in advanced prostate cancer. *Expert Opin Investig Drugs.* 2008;17:23–29.
6. Baguley BC, Siemann DW. Temporal aspects of the action of ASA404 (vadimezan; DMXAA). *Expert Opin Investig Drugs.* 2010;19:1413–1425.
7. Murata R, Overgaard J, Horsman MR. Comparative effects of combretastatin A-4 disodium phosphate and 5,6-dimethylxanthenone-4-acetic acid on blood perfusion in a murine tumour and normal tissues. *Int J Radiat Biol.* 2001;77:195–204.
8. Siim BG, Laux WT, Rutland MD, Palmer BN, Wilson WR. Scintigraphic imaging of the hypoxia marker ^{99m}technetium-labeled 2,2′-(1,4-diaminobutane)bis (2-methyl-3-butanone) dioxime (^{99m}Tc-labeled HL-91; Prognox): noninvasive detection of tumor response to the antivascular agent 5,6-dimethylxanthenone-4-acetic acid. *Cancer Res.* 2000;60:4582–4588.
9. McPhail LD, McIntyre DJ, Ludwig C, et al. Rat tumor response to the vascular-disrupting agent 5,6-dimethylxanthenone-4-acetic acid as measured by dynamic contrast-enhanced magnetic resonance imaging, plasma 5-hydroxyindoleacetic acid levels, and tumor necrosis. *Neoplasia.* 2006;8:199–206.
10. Chaplin DJ, Hill SA. The development of combretastatin A4 phosphate as a vascular targeting agent. *Int J Radiat Oncol Biol Phys.* 2002;54:1491–1496.
11. Eisenhauer EA, Therasse P, Bogaerts J, et al. New response evaluation criteria in solid tumours: revised RECIST guideline (version 1.1). *Eur J Cancer.* 2009;45:228–247.
12. Therasse P, Arbuck SG, Eisenhauer EA, et al. New guidelines to evaluate the response to treatment in solid tumors. European Organization for Research and Treatment of Cancer, National Cancer Institute of the United States, National Cancer Institute of Canada. *J Natl Cancer Inst.* 2000;92:205–216.
13. Wahl RL, Jacene H, Kasamon Y, Lodge MA. From RECIST to PERCIST: evolving considerations for PET response criteria in solid tumors. *J Nucl Med.* 2009;50(suppl 1):122S–150S.
14. Galbraith SM, Rustin GJ, Lodge MA, et al. Effects of 5,6-dimethylxanthenone-4-acetic acid on human tumor microcirculation assessed by dynamic contrast-enhanced magnetic resonance imaging. *J Clin Oncol.* 2002;20:3826–3840.
15. Seshadri M, Toth K. Acute vascular disruption by 5,6-dimethylxanthenone-4-acetic acid in an orthotopic model of human head and neck cancer. *Transl Oncol.* 2009;2:121–127.
16. Wilson WR, Li AE, Cowan DS, Siim BG. Enhancement of tumor radiation response by the antivascular agent 5,6-dimethylxanthenone-4-acetic acid. *Int J Radiat Oncol Biol Phys.* 1998;42:905–908.
17. Murata R, Siemann DW, Overgaard J, Horsman MR. Improved tumor response by combining radiation and the vascular-damaging drug 5,6-dimethylxanthenone-4-acetic acid. *Radiat Res.* 2001;156:503–509.
18. McKeage MJ, Von Pawel J, Reck M, et al. Randomised phase II study of ASA404 combined with carboplatin and paclitaxel in previously untreated advanced non-small cell lung cancer. *Br J Cancer.* 2008;99:2006–2012.
19. Mees G, Dierckx R, Vangestel C, Van de Wiele C. Molecular imaging of hypoxia with radiolabelled agents. *Eur J Nucl Med Mol Imaging.* 2009;36:1674–1686.
20. Cher LM, Murone C, Lawrentschuk N, et al. Correlation of hypoxic cell fraction and angiogenesis with glucose metabolic rate in gliomas using ^{18}F-fluoromisonidazole, ^{18}F-FDG PET, and immunohistochemical studies. *J Nucl Med.* 2006;47:410–418.
21. Koh WJ, Bergman KS, Rasey JS, et al. Evaluation of oxygenation status during fractionated radiotherapy in human nonsmall cell lung cancers using [F-18]fluoromisonidazole positron emission tomography. *Int J Radiat Oncol Biol Phys.* 1995;33:391–398.
22. Tjuvajev JG, Avril N, Oku T, et al. Imaging herpes virus thymidine kinase gene transfer and expression by positron emission tomography. *Cancer Res.* 1998;58:4333–4341.
23. Lim JL, Berridge MS. An efficient radiosynthesis of [^{18}F]fluoromisonidazole. *Appl Radiat Isot.* 1993;44:1085–1091.
24. Nahmias C, Wahl LM. Reproducibility of standardized uptake value measurements determined by ^{18}F-FDG PET in malignant tumors. *J Nucl Med.* 2008;49:1804–1808.
25. Russell J, Carlin S, Burke SA, Wen B, Yang KM, Ling CC. Immunohistochemical detection of changes in tumor hypoxia. *Int J Radiat Oncol Biol Phys.* 2009;73:1177–1186.
26. Li XF, Carlin S, Urano M, Russell J, Ling CC, O'Donoghue JA. Visualization of hypoxia in microscopic tumors by immunofluorescent microscopy. *Cancer Res.* 2007;67:7646–7653.
27. Rajendran JG, Krohn KA. Imaging hypoxia and angiogenesis in tumors. *Radiol Clin North Am.* 2005;43:169–187.
28. Seshadri M, Bellnier DA, Cheney RT. Assessment of the early effects of 5,6-dimethylxanthenone-4-acetic acid using macromolecular contrast media-enhanced magnetic resonance imaging: ectopic versus orthotopic tumors. *Int J Radiat Oncol Biol Phys.* 2008;72:1198–1207.
29. Seshadri M, Ciesielski MJ. MRI-based characterization of vascular disruption by 5,6-dimethylxanthenone-acetic acid in gliomas. *J Cereb Blood Flow Metab.* 2009;29:1373–1382.
30. Cho H, Ackerstaff E, Carlin S, et al. Noninvasive multimodality imaging of the tumor microenvironment: registered dynamic magnetic resonance imaging and positron emission tomography studies of a preclinical tumor model of tumor hypoxia. *Neoplasia.* 2009;11:247–259.
31. Wang W, Georgi JC, Nehmeh SA, et al. Evaluation of a compartmental model for estimating tumor hypoxia via FMISO dynamic PET imaging. *Phys Med Biol.* 2009;54:3083–3099.
32. Wang W, Lee NY, Georgi JC, et al. Pharmacokinetic analysis of hypoxia ^{18}F-fluoromisonidazole dynamic PET in head and neck cancer. *J Nucl Med.* 2010;51:37–45.
33. Troost EG, Laverman P, Kaanders JH, et al. Imaging hypoxia after oxygenation-modification: comparing [^{18}F]FMISO autoradiography with pimonidazole immunohistochemistry in human xenograft tumors. *Radiother Oncol.* 2006;80:157–164.

Downloaded from jnm.snmjournals.org by on March 11, 2017. For personal use only.

JNM The Journal of NUCLEAR MEDICINE

^{18}F-Fluromisonidazole PET Imaging as a Biomarker for the Response to 5,6-Dimethylxanthenone-4-Acetic Acid in Colorectal Xenograft Tumors

Christoph Oehler, Joseph A. O'Donoghue, James Russell, Pat Zanzonico, Sylvie Lorenzen, C. Clifton Ling and Sean Carlin

J Nucl Med. 2011;52:437-444.
Published online: February 14, 2011.
Doi: 10.2967/jnumed.110.081372

This article and updated information are available at:
http://jnm.snmjournals.org/content/52/3/437

Information about reproducing figures, tables, or other portions of this article can be found online at:
http://jnm.snmjournals.org/site/misc/permission.xhtml

Information about subscriptions to JNM can be found at:
http://jnm.snmjournals.org/site/subscriptions/online.xhtml

The Journal of Nuclear Medicine is published monthly.
SNMMI | Society of Nuclear Medicine and Molecular Imaging
1850 Samuel Morse Drive, Reston, VA 20190.
(Print ISSN: 0161-5505, Online ISSN: 2159-662X)

© Copyright 2011 SNMMI; all rights reserved.

SNMMI SOCIETY OF NUCLEAR MEDICINE AND MOLECULAR IMAGING